# The gaseous plasmonic response of a one-dimensional photonic crystal composed of striated plasma layers

Cite as: Phys. Plasmas **25**, 031902 (2018); https://doi.org/10.1063/1.5018422
Submitted: 06 December 2017 . Accepted: 11 February 2018 . Published Online: 20 March 2018

B. Wang, F. Righetti, and M. A. Cappelli

# The gaseous plasmonic response of a one-dimensional photonic crystal composed of striated plasma layers

B. Wang, F. Righetti, and M. A. Cappelli[a)]
*Department of Mechanical Engineering, Stanford University, Stanford, California 94305, USA*

(Received 6 December 2017; accepted 11 February 2018; published online 20 March 2018)

We present simulations of the response of a one-dimensional striated plasma slab to incident electromagnetic waves that span regions both above and below the plasma frequency, $\omega_p$. Photonic bandgap modes are present throughout these regions, and volume and surface plasmon modes facilitate the response below $\omega_p$, where the dielectric constant, $\varepsilon_p < 0$. In the vicinity of $\omega_p$, most apparently, when $\omega_p$ is in proximity of the lattice frequency, there is a feature for transverse magnetic (TM) polarization that is associated with the emergence of new dispersion branches. Also for TM polarization, a very low frequency mode emerges outside of the light line. Both these features are plasmonic and are attributed to the excitation of symmetric and asymmetric surface plasmon polaritons (SPPs) at the plasma-dielectric interface of the multi-layer plasma slabs. The features seen in the bandgap maps near $\omega_p$ reveal the possible presence of Fano resonances between the symmetric branch of the SPP and the Bragg resonance as a narrow stop band (anti-node) is superimposed on the otherwise broad transmission band seen for transverse-electric polarization. We provide renderings that allow the visualization of where the transmission bands are and compute the transmittance and reflectance to facilitate the design and interpretation of experiments. The transmission bands associated with photonic bandgap modes above the plasma frequency are rather broad. The plasmonic modes, i.e., those associated with $\varepsilon_p \leq 0$, can be quite narrow and are tuned by varying the plasma density, affording an opportunity for the application of these structures as ultra-narrow tunable microwave transmission filters. *Published by AIP Publishing.*
https://doi.org/10.1063/1.5018422

## I. INTRODUCTION

A photonic crystal (PC) is a generally passive artificially engineered material that selectively transmits or reflects electromagnetic (EM) waves over a designed range of frequencies.[1] The associated EM passbands or bandgaps arise due to destructive and constructive Bragg scattering interferences within the periodic structure. A plasma photonic crystal (PPC)[2–6] is a type of PC that allows for the reconfiguration of its EM response through the use of controllable gaseous plasma elements. The simplest PPCs consist of one-dimensional (1D) striated plasma-vacuum or plasma-dielectric layers with repeating dimensions that are on the order of the wavelength of the EM wave.[2] Two-dimensional (2D) and three-dimensional (3D) PPCs would be stand-alone higher dimensionality plasma structures[4] or would incorporate repeating plasma structures into a 2D or 3D dielectric scaffold. As in passive PCs, PPCs can be functionalized by incorporating defects into their structure. Also, otherwise passive PCs can be functionalized by incorporating plasma defects, resulting in novel devices such as tunable bandpass filters[6] and power limiters.[7]

The challenge faced in designing PC devices is in choosing the configurations and properties of the materials that determine the location, width, and depth of the bandgaps. This becomes particularly more difficult when plasmas are incorporated, as plasmas have a frequency-dependent dielectric constant, $\varepsilon_p$, that varies strongly in the vicinity of the plasma frequency, $\omega_p$. The region of EM wave propagation corresponding to frequencies below $\omega_p$ is the one that is often overlooked in the discussion about PPC performance. However, we have shown in previous work that in finite-sized 2D plasma photonic crystals,[5] the strongest stop band is due to plasmonic modes at frequencies $\omega < \omega_p$. As we will show below, plasmon oscillations play a critical role in the formation of stop and transmission bands near and below the plasma frequency—features that are not seen in all-dielectric PCs. The features in the vicinity of $\omega_p$ are also highly tunable by varying the plasma density, $n_e$. PPCs therefore afford the possibility of integrating tunable plasmonics into microwave devices to control EM propagation, defining an emerging field of plasma physics that one might describe as "gaseous plasmonics".

As mentioned above, $\varepsilon_p$ depends on $\omega_p$, which is a function of the electron density, $n_e$. The plasma frequency is the frequency of collective electron oscillations, sometimes referred to as "bulk" or "volume" plasmons, excited when the plasma is subjected to disturbances such as an incident oscillating electric field. When the plasma is collisional (electron collision frequency, $\nu$), the dielectric constant is complex and can be represented by the Drude model, given by

[a)]Electronic mail: cap@stanford.edu

$$\varepsilon_p = 1 - \frac{\omega_p^2}{\omega(\omega + i\nu)}. \quad (1)$$

For a collisionless plasma ($\nu = 0$), $\varepsilon_p$ takes on values near unity well above $\omega_p$, crosses through zero at $\omega_p$, and then becomes strongly negative just below $\omega_p$. A graph of the variation of $\varepsilon_p$ with frequency is shown in Fig. 1 for $\nu = 0$ and a range of values of $\omega_p$. For convenience, the frequencies in this figure have been non-dimensionalized by the PPC lattice frequency, which is the frequency associated with the free-space propagation of an EM wave of speed $c$ and wavenumber corresponding to the 1D photonic crystal lattice parameter, $\Lambda$. We see from Eq. (1) as well as from the figure that $\varepsilon_p$ is strongly negative for frequencies not too far below $\omega_p$. We also see that a plasma has a limiting positive dielectric constant of $\varepsilon_{pmax} = 1$, resulting in a permittivity equal to that of free space, $\varepsilon_o$. The plasma frequency is defined as $\omega_p = \sqrt{n_e e^2/m_e\varepsilon_o}$. Here, $e$ and $m_e$ are the electron charge and mass, respectively. A variable electron density allows for $\omega_p$ and hence $\varepsilon_p$ to be tuned. When plasma slabs are combined with dielectric slabs of dielectric constant $\varepsilon_b$, a PPC can result in a device with relatively deep photonic bandgaps which broaden (and shift slightly towards higher frequency) with increasing $n_e$. In contrast, we show below that there are strong plasmonic reflection/transmission features near $\omega_p$ which are therefore strongly tunable by varying the plasma density.

This paper focuses on the transmission properties of 1D collisionless, non-magnetized PPCs although some features described here are also expected for PPCs of higher dimensionality. Previous studies have presented theoretical analyses of both non-magnetized[8–11] and magnetized[11–13] 1D PPC performances. In this paper, we present bandgap diagrams which can be used to facilitate the PPC design for a desired response. For frequencies above the plasma frequency, the plasma behaves as a simple dielectric with variable permittivity. Transmission band maps appear in many ways similar to those of conventional 1D PCs. However, at frequencies below the plasma frequency, the transmission through the plasma slabs is facilitated by evanescent wave coupling, similar to what is seen in 1D metal-dielectric layered structures[14–16] and first discussed in reference to plasma photonic crystals by Sakai and Tachibana.[17] The features appearing in this regime are plasmonic, i.e., associated with either bulk or surface plasmon oscillations. It is well known that for $\omega < \omega_p$, EM waves incident onto a semi-infinite plasma slab result in exponentially damped EM fields (see the top image of Fig. 2), with a decay length that can be sub-wavelength in scale. This results in a reflection of waves incident on a dielectric-plasma interface as $\varepsilon_p < 0$, and the refractive index of the plasma, $n_p = \sqrt{\varepsilon_p}$, is imaginary. At oblique incidence, with polarization such that there is an electric field component normal to the plane of the slab, it can excite surface plasmon polaritons (SPPs), which are propagating EM waves, the amplitudes of which decay as evanescent fields away from the interface. For a finite thickness plasma slab, evanescent fields can "tunnel" through (lower image of Fig. 2), resulting in partial transmission of the field. As we show below, this transmission and subsequent reflection/transmission from the other slabs in the PPC result in resonances or field concentrations within the dielectric structures with amplitudes greater than those of the incident fields. Closely related SPP-facilitated stop and pass bands appear for oblique angles of incidence in transverse magnetic (TM) polarization conditions. New transmission modes appear within photonic bandgaps, and new stop bands appear within pass bands at frequencies near $\omega_p$.[18] The structure of the transmittance spectra in the vicinity of $\omega_p$ when the plasma frequency is in proximity to the lattice frequency is attributed to the lattice or Fano resonance associated with the interference of the surface waves with the broader Bragg resonance driven by the external EM field.[19] We examine the field

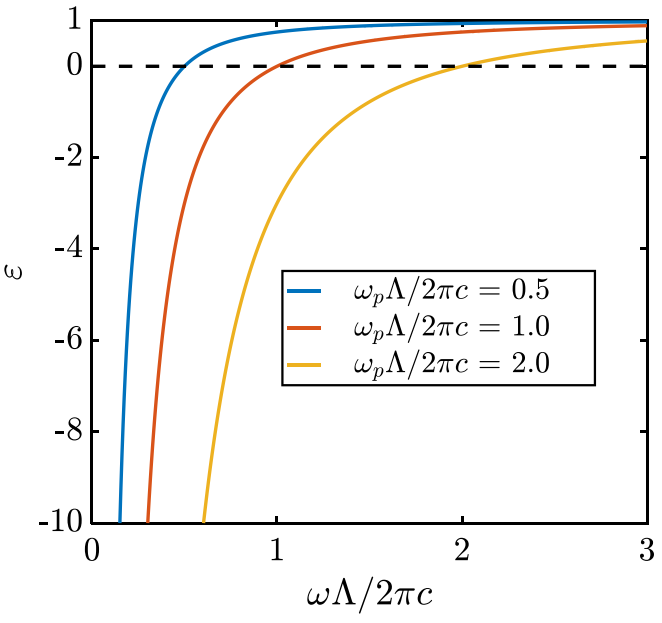


FIG. 1. Drude model for the non-dimensionalized frequency variation in the dielectric constant, $\varepsilon_p$, for three values of $\omega_p\Lambda/2\pi$ and $\nu = 0$.

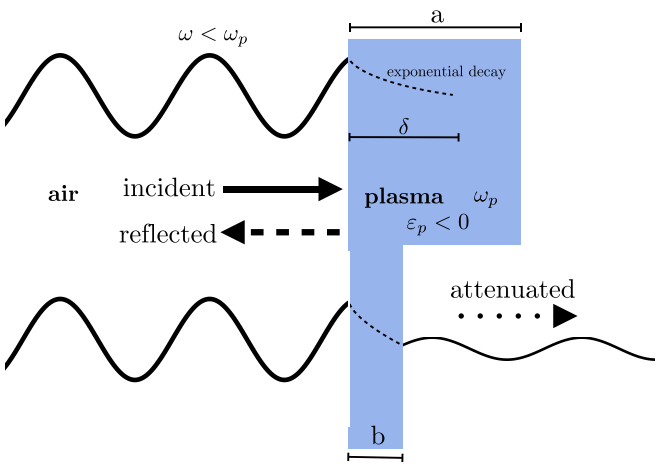


FIG. 2. Diagram illustrating an incident EM wave of frequency, $\omega$, onto a plasma slab with plasma frequency, $\omega_p$. For $\omega < \omega_p$, $\varepsilon_p < 0$ and the field decays exponentially as an evanescent wave. If the plasma thickness is greater than the decay length of the wave (top illustration), then there is little or no transmitted wave. If the plasma thickness is less than the decay length of the wave, then there is a tunneling of the EM wave through the plasma.

distribution within the crystal for these plasmonic modes, the stop and pass band properties of which can be very narrow in frequency space.

Reports on the experimental generation of 1D plasma photonic crystals have employed gas discharges in plasma formation.[10,20,21] Low collisionality, low density plasmas formed by either electrical or optical discharges in low pressure gases have plasma densities ranging from $n_e = 10^{17}$ m$^{-3}$ to $n_e = 10^{20}$ m$^{-3}$ with corresponding plasma frequencies of 2.8 GHz to 90 GHz, spanning a range of EM spectra of significant technological relevance. In a previous study, we have experimentally confirmed the bandgap characteristics of a 2D plasma photonic crystal constructed from an array of discharge tubes with the response in the 2–10 GHz range.[5] In that study, tuning was achieved by varying the plasma density via control of discharge current. As we further this 2D technology and also study the potential development of 1D plasma arrays consisting of plasma slabs, the availability of resources such as bandgap diagrams for the design of PPCs would be of much value.

Transfer matrix formalism (TMF) is commonly used for computing the bandgap and dispersion diagrams of conventional 1D photonic crystals.[22] The dispersion diagrams for 1D plasma photonic crystals generated using the TMF have been published.[2] While dispersion diagrams help in understanding regimes of transmission and attenuation, their complexity, particularly at higher frequencies, make interpretation cumbersome. Bandgap maps afford a straightforward alternative for visualizing the effects of how array and plasma parameters affect bandgap locations and size. Below, we present bandgap maps for two different PPC constructions, both of which may be conceivably generated in the laboratory. One case is a configuration in which a dielectric material is inserted between uniform plasma density slabs, while the other is with the uniform density plasma slabs separated by vacuum (or unionized vapor). It is noteworthy that the generation of uniform slabs is a challenge in itself, and so, the results described below should be seen as idealized cases, with bandgap boundaries degraded somewhat by non-uniformities within the slabs.

## II. THEORETICAL MODEL

Figure 3 shows the 1-D dielectric photonic crystal slab considered in this analysis with plasma of thickness $a$ and dielectric of thickness $b$ and with a lattice constant $\Lambda = a + b$. Normal incident, transverse electric (TE), and transverse magnetic (TM) polarizations are considered. For all calculated bandgap maps, dispersion diagrams, and transmittance spectra, frequencies are non-dimensionalized by the lattice frequency $2\pi c/\Lambda$ (here, c is the speed of EM waves in free space) and length scales such as the thickness of the plasma slab, $a$, are normalized by $\Lambda$. The ratio of $a/\Lambda$ represents the plasma fill fraction.

Determining the EM wave propagation characteristics requires the complex elements of the ABCD matrix.[22] The reflectance of a 1-D photonic crystal is then determined from

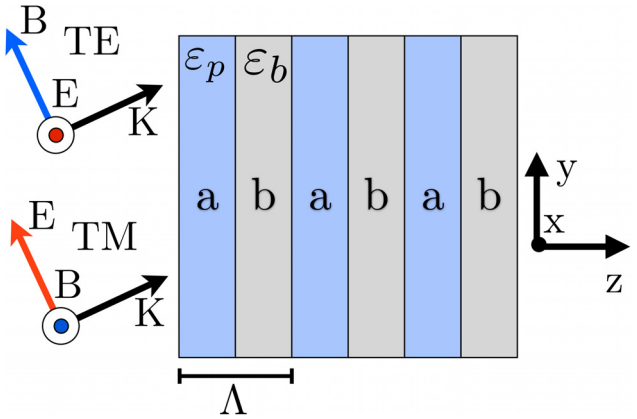


FIG. 3. 1-D dielectric photonic crystal slab with plasma thickness a, dielectric thickness b, and lattice constant Λ. TE and TM polarization field orientations are shown.

$$|r_N|^2 = \frac{|C|^2}{|C|^2 - (\sin K\Lambda / \sin NK\Lambda)^2}. \tag{2}$$

Here, $N$ is the total number of lattice unit cells that make up the thickness of the 1D array and $K = (1/\Lambda)\cos^{-1}[\frac{1}{2}(A+D)]$ is the Bloch wavenumber, which characterizes the wave dispersion. The transmittance of the photonic crystal is $|t_n|^2 = 1 - |r_n|^2$ in the absence of electron collisional damping.

For TE polarization, the elements of the ABCD matrix are

$$A = \left[\cos k_{pz}a - \frac{1}{2}i\left(\frac{k_{pz}}{k_{bz}} + \frac{k_{bz}}{k_{pz}}\right)\sin k_{pz}a\right]e^{-ik_{bz}b}, \tag{3}$$

$$B = \left[-\frac{1}{2}i\left(\frac{k_{pz}}{k_{bz}} - \frac{k_{bz}}{k_{pz}}\right)\sin k_{pz}a\right]e^{ik_{bz}b}, \tag{4}$$

$$C = \left[\frac{1}{2}i\left(\frac{ik_{pz}}{k_{bz}} - \frac{k_{bz}}{ik_{pz}}\right)\sin k_{pz}a\right]e^{-ik_{bz}b}, \tag{5}$$

$$D = \left[\cos k_{pz}a + \frac{1}{2}i\left(\frac{k_{pz}}{k_{bz}} + \frac{k_{bz}}{k_{pz}}\right)\sin k_{pz}a\right]e^{ik_{bz}b}, \tag{6}$$

where $k_{bz} = \left(\frac{\omega^2}{c^2}\varepsilon_b - k_y^2\right)^{1/2}$ and $k_{pz} = \left[\frac{\omega^2}{c^2}\left(1 - \frac{\omega_p^2}{\omega^2}\right) - k_y^2\right]^{1/2}$.

For TM polarization, the ABCD matrix elements are

$$A = \left[\cos k_{pz}a - \frac{1}{2}i\left(\frac{n_p^2 k_{bz}}{n_b^2 k_{pz}} + \frac{n_b^2 k_{pz}}{n_p^2 k_{bz}}\right)\sin k_{pz}a\right]e^{-ik_{bz}b}, \tag{7}$$

$$B = \left[-\frac{1}{2}i\left(\frac{n_p^2 k_{bz}}{n_b^2 k_{pz}} - \frac{n_b^2 k_{pz}}{n_p^2 k_{bz}}\right)\sin k_{pz}a\right]e^{ik_{bz}b}, \tag{8}$$

$$C = \left[\frac{1}{2}i\left(\frac{n_p^2 k_{bz}}{n_b^2 k_{pz}} - \frac{n_b^2 k_{pz}}{n_p^2 k_{bz}}\right)\sin k_{pz}a\right]e^{-ik_{bz}b}, \tag{9}$$

$$D = \left[\cos k_{pz}a + \frac{1}{2}i\left(\frac{n_p^2 k_{bz}}{n_b^2 k_{pz}} + \frac{n_b^2 k_{pz}}{n_p^2 k_{bz}}\right)\sin k_{pz}a\right]e^{ik_{bz}b}. \tag{10}$$

In the above matrix elements, $k_y$ is the component wavenumber in the plane of the 1D slab (this defines the incidence angle, with $k_y = 0$ equal to the normal incidence case where TM and TE modes are degenerate), $n_b = \sqrt{\varepsilon_b}$ is the

dielectric slab refractive index (assumed real), and $n_p = \sqrt{1 - \frac{\omega_p^2}{\omega^2}}$ is the complex refractive index of the plasma.

The dispersion relation is solved for specified values of the dielectric constant, $\varepsilon_b$, and a range of field and plasma frequencies, $\omega$ and $\omega_p$, respectively. The band edges can be determined when the Bloch wavenumber $K = N\pi/\Lambda$, resulting in a reflectance

$$|r_N|^2_{edge} = \frac{|C|^2}{|C|^2 + (1/N)^2}. \tag{11}$$

In the limit of $N \to \infty$, the band edge reflectance approaches unity. For a finite $N$, between the bandgaps, there are $N - 1$ nodes where the reflectance goes to zero[22] or the transmittance goes to one.

## III. RESULTS AND DISCUSSION

### A. Normal incidence

Lattice bandgap maps for the normal incidence properties of a 1D collisionless plasma photonic crystal and $N = \infty$ show several interesting characteristics. Figure 4 shows the lattice bandgap map of a 1-D plasma photonic crystal for vacuum ($\varepsilon_b = 1$) and dielectric ($\varepsilon_b = 5$) layers between the plasma slabs [Figs. 4(a) and 4(b), respectively] and for $\omega_p = 2\pi$ c/$\Lambda$, the lattice frequency. For both cases, the lowest frequency stop band is due to the plasma cut-off commonly seen with a plasma medium, as evidenced by the extension of this region as far up as the plasma frequency when the plasma slab thickness $a \to \Lambda$. This cut-off band closes, i.e., decreases in width as the plasma size decreases, with the upper boundary shifting downwards, resulting in transmission below the plasma frequency due to the tunneling of the evanescent waves. Some researchers[23] have interpreted this as a reduction in the effective plasma frequency, $\omega_{p_{eff}}$, with decreased fill fraction, $a/\Lambda$, which, for small fill fractions, $\omega_{p_{eff}} \approx (a/\Lambda\varepsilon_d)^{1/2}\omega_p$. For a particular value of the EM wave frequency, the upper boundary of this cut-off band shifts towards larger values of $a/\Lambda$ for the higher dielectric case, as the wavelengths are longer within the dielectric than in vacuum. The transmission between the cut-off and the first bandgap as well as between higher bandgaps below $\omega_p$ is facilitated by the evanescent wave coupling of the incident fields into propagation modes in the dielectric layers.

The first photonic bandgap forms when waves destructively interfere as a result of scattering from the dielectric and plasma interfaces. For the vacuum case, the first bandgap emerges at a frequency equal to half the lattice frequency (as $a/\Lambda \to 0$), as expected for a 1D photonic crystal comprising thin slabs in vacuum. This band thickness increases in width as the plasma size increases until around $a/\Lambda = 0.5$ and then begins to decrease towards zero thickness as $a/\Lambda$ approaches unity. Of course, for $a = \Lambda$, there is propagation at all frequencies above the plasma frequency. The first bandgap emerges at lower frequencies for the high dielectric constant case and the mode density over a fixed range of frequencies is higher—a consequence of the shorter wavelengths within the dielectric; however, they terminate, as expected, at the same frequency as $a \to \Lambda$ since the presence of the dielectric plays a lesser role. In both cases, the pattern continues with higher frequency bands. For the vacuum case, second and third bands lie above the plasma frequency since in the absence of a plasma, the bands emerge at harmonics of the first band. This is in contrast to the high index dielectric, which has several bands emerging below the plasma frequency. In both cases, these bands diminish in width with frequency as the index contrast diminishes since the plasma dielectric constant approaches unity with increasing frequency above $\omega_p$. Depicted in this way, we are also able to visualize the nodes in any particular gap which appear at characteristic values of $a/\Lambda$. These are a consequence of the Bragg interferences which appear with varying plasma slab thicknesses and the number of which increases with increasing frequency due to the shorter wavelength within the vacuum and slabs. Finally, because of the higher mode density within a fixed frequency range for the $\varepsilon_b = 5$ case as $a/\Lambda \to 0$, the bands steepen with increasing plasma slab thickness $a/\Lambda$.

Understanding the relationship between the normal incidence dispersion and transmittance spectra for vacuum is important in understanding the dynamics of the transmission (or Bragg resonance) modes. The dispersion relationships and transmittance are shown in Fig. 5 for $a/\Lambda = 0.1$, 0.5, and 0.9, $N = 20$, and $\varepsilon_b = 1$. For all three $a/\Lambda$ cases, we see that

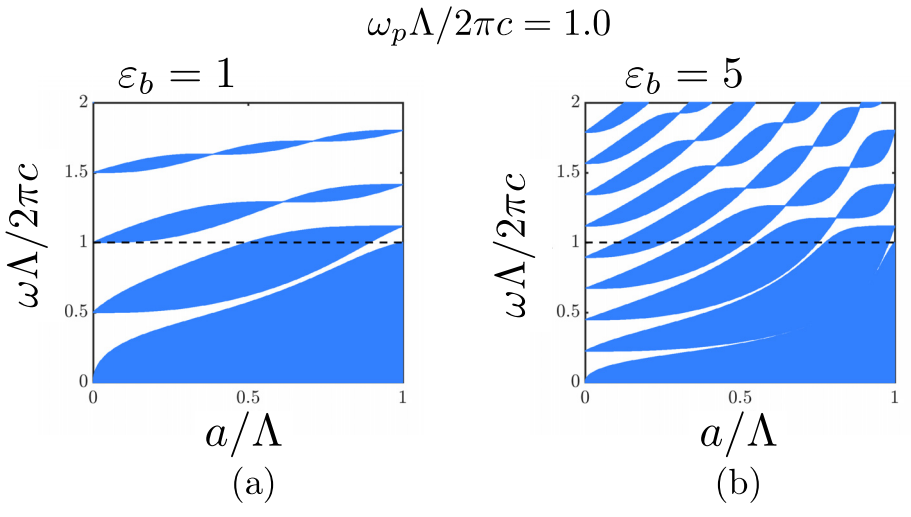


FIG. 4. Bandgap frequency vs. plasma thickness at normal incidence for a 1D plasma photonic crystal with dielectric layers consisting of: (a) vacuum with $\varepsilon_b = 1$ and (b) a dielectric with $\varepsilon_b = 5$. All colored (solid) regions are frequencies that are in a bandgap. The horizontal dotted line denotes the plasma frequency, with $\omega_p\Lambda/2\pi c = 1$ and $N = \infty$.

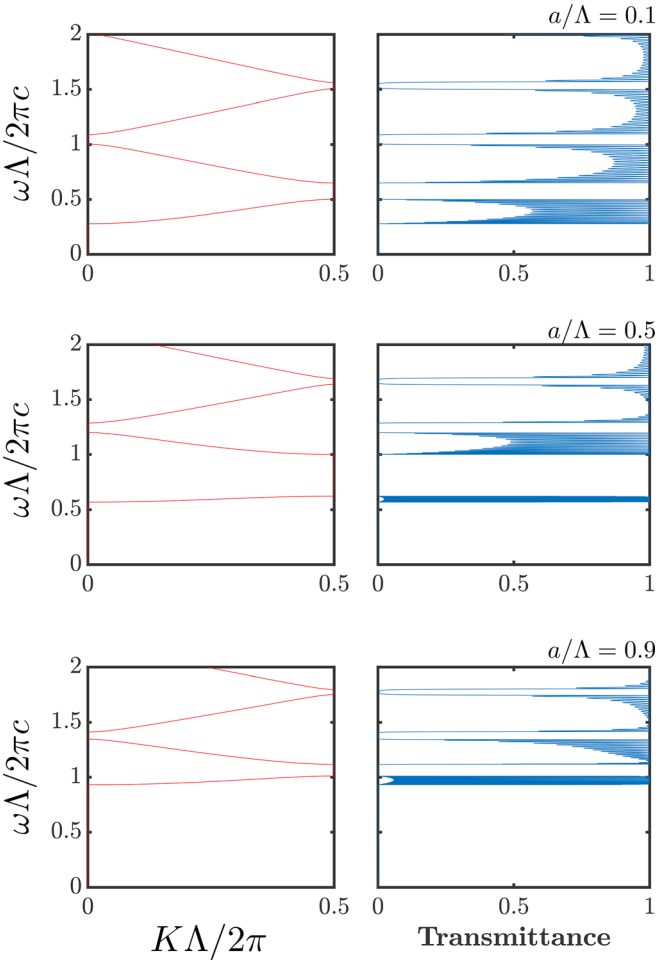


FIG. 5. Dispersion diagrams (left) and transmittance spectra (right) for a 1D plasma photonic crystal in vacuum at normal incidence for N = 20 and $\omega_p\Lambda/2\pi c = 1$ for $a/\Lambda = 0.1$, 0.5, and 0.9.

the bandgaps above the effective plasma frequency have characteristic pass bands found in all-dielectric 1D photonic crystals. The predicted transmission bands below the plasma frequency for intermediate values of $a/\Lambda$ are quite narrow, reflecting a diminishing group velocity of this plasmonic branch (since $\varepsilon_p < 0$), consistent with the bandgap maps in Fig. 4(a). The near-zero group velocity suggests EM wave energy accumulation within the structure due to EM field trapping resonances.

We can gain further insight into the behavior of the PPC in the vicinity of the dispersion branch near $\omega_{p_{eff}}$ by examining the fields within the multilayer structure. While in principle, the transfer matrix method enables the calculation of the fields within the plasma and dielectric layers, we use the Stanford Stratified Structure Solver ($S^4$), which employs the Fourier Modal Method (FMM) to solve for the wave field eigenvalues.[24] An example calculation of the normal incidence ($N = 20$ and $a/\Lambda = 0.1$, 0.5, 0.9 cases) transmission (top panels) and internal wave fields (lower panels) is given in Fig. 6. The lower panels present the square of the modulus of the E-field (in blue or dashed line) and the H-field (in red or solid line) for frequencies corresponding to the vertical lines in the upper panels, i.e., centered at three of the $N - 1$ expected transmission peaks within the first transmission band in the vicinity of $\omega_{p_{eff}}$. Note that the fields are normalized to the incident field values. In the lower panels, features are shown for portions or all the $N = 20$ lattice cells, to capture the field envelopes that repeat along the direction of propagation.

For all cases, the electric fields within the plasma layers decay exponentially, an expected behavior within the plasma layers since $\omega < \omega_p$. We see that within a particular transmission band, there is significant field variation across the $N - 1$ transmission peaks. In almost all cases, the fields within the dielectric are amplified, i.e., the magnitude is much greater than that of the incident field indicative of resonances which are due to the confinement of the EM waves within the dielectric layer (vacuum in this case). In some cases, extremely high field amplifications are seen, as high as $\approx 10^3$ for $a/\Lambda \approx 0.5$. This results in inter-band transmission peaks of extremely high $Q$, as seen in the top panels of the figure. Such high-$Q$ transmission resonances are potentially useful as tunable microwave filters as the location of the pass band is varied by changing the plasma density. It is noteworthy that the field amplification within the transmission peaks in the pass bands above $\omega_{p_{eff}}$ is of order unity (not shown here). The high $Q$ plasmonic transmission bands are due to the evanescent wave coupling to the propagating modes. This is also seen in 1D metal-dielectric PCs,[16] with the difference being that these resonances are tunable, whereas in metals, they are not.

Figure 7 shows the normal incidence gap dependence on plasma frequency for $a/\Lambda = 0.1$ and $a/\Lambda = 0.5$ and $N = \infty$. In this figure, transmission bands are plasmonic for frequencies below the line defining $\omega = \omega_p$. In general, for $a/\Lambda = 0.1$, the bandgaps increase in width with increasing $n_e$, resulting in a concomitant reduction in the width of the transmission bands. The upper boundary of the cut-off band, which defines $\omega_{p_{eff}}$, also increases with $n_e$. This boundary represents the lower frequency limit of the first transmission band, which encompasses the $N - 1$ high -$Q$ transmission peaks described for $\varepsilon_b = 1$ in the center panels of Fig. 6. As we can see from Fig. 7, the upper boundary of this transmission band (coinciding with the lower boundary of the first bandgap) is not a strong function of $n_e$, resulting in a transmission band that becomes narrower with increasing $n_e$ and therefore a decreased spacing between the $N - 1$ transmission modes. Tunability is therefore strongest for the lowest frequency transmission mode within the manifold. The $\varepsilon_b = 5$ case has similar features but compressed, resulting in a higher mode density due to the shorter wavelengths within the dielectric. The features for the larger plasma fill fraction case are more complex. Again, transmission bands below the line defining $\omega = \omega_p$ are coupled through evanescent waves in the plasma and are therefore plasmonic. At higher plasma densities, these transmission bands are quite narrow. At even higher fill fractions, the region below the plasma frequency will eventually come close to transmission as the slab becomes almost entirely plasma-filled.

### B. Oblique incidence

We now consider the oblique incidence response of the PPC. To do so, we differentiate between TE and TM

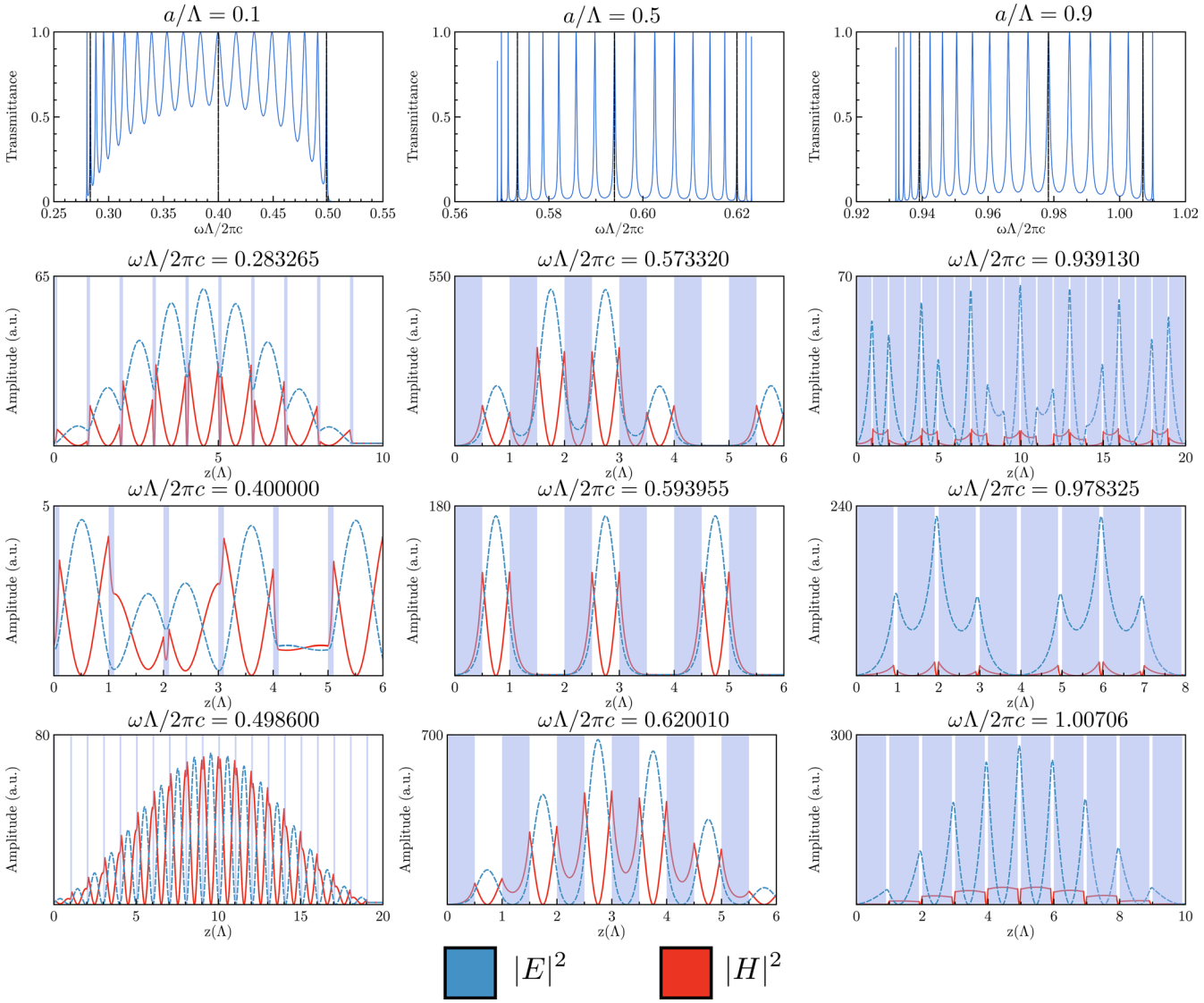


FIG. 6. Zoomed in transmittance spectra (top) showing inter-band modes for a 1D plasma photonic crystal in vacuum at normal incidence for N = 20 and $\omega_p\Lambda/2\pi c = 1$ for $a/\Lambda = 0.1$, 0.3, and 0.9. Cross-sectional electric and magnetic fields are shown for specific frequencies of interest indicated by the vertical lines in the transmittance spectra calculated using S4.

polarizations, as shown in Fig. 3. We begin by recalculating the bandgap maps in Fig. 4 for oblique incidence conditions defined by a finite value of the $y$-component wavevector, $k_y$. Figure 8 shows cases for $k_y\Lambda/2\pi = 0.1$ and 0.3. The horizontal dashed line denotes the plasma frequency since for these calculations, we take $\omega_p\Lambda/2\pi c = 1$. Note that a horizontal solid black line in these figures distinguishes simulations for conditions of propagation within (above the line) and outside (below the line) the light line defined by $\omega\Lambda/2\pi c = 0.1$, 0.3 since oblique incidence coupling from vacuum requires $k_y c/\omega < 1$. The propagation characteristics outside of the light line are included as methods exist for the coupling of EM waves into lower-index materials. As we can see from the top panels, the TE cases are unremarkable, as they are similar in several ways to the zero-incidence angle case, with the exception of shifts associated with reduced values of $k_z$-component wavenumbers due to the non-zero $k_y$. The TM case has additional features in the vicinity of the plasma frequency, $\omega_p\Lambda/2\pi c = 1$. For example, at low and high fill fractions, we see the emergence of a narrow stop band within the photonic pass bands. The fact that these bands appear in the vicinity of $\omega_p$ suggests that these bands are associated with the plasmonic resonances of the plasma slabs, particularly in the vicinity of $\varepsilon_p \approx 0$ (epsilon-near-zero or ENZ) where the refractive index of the plasma is near zero. The emergence of these features, unique to TM polarization, was first observed in simulations of 1D plasma PCs by Shiveshwari[18] although several years earlier, they were also predicted to appear in 1D metamaterial photonic crystals in which one of the repeating layers consists of either a zero permeability or zero permittivity material.[25] In these previous discoveries, they are described as "non-Bragg" gaps, the physical mechanism of which was not discussed. We attribute these stop bands to "lattice" or Fano resonances resulting from the interference between the Bragg resonance at the lattice frequency and the symmetric branch of surface plasmon polaritons (SPPs) propagating along the y-direction at the boundaries of the plasma slabs excited by the incident

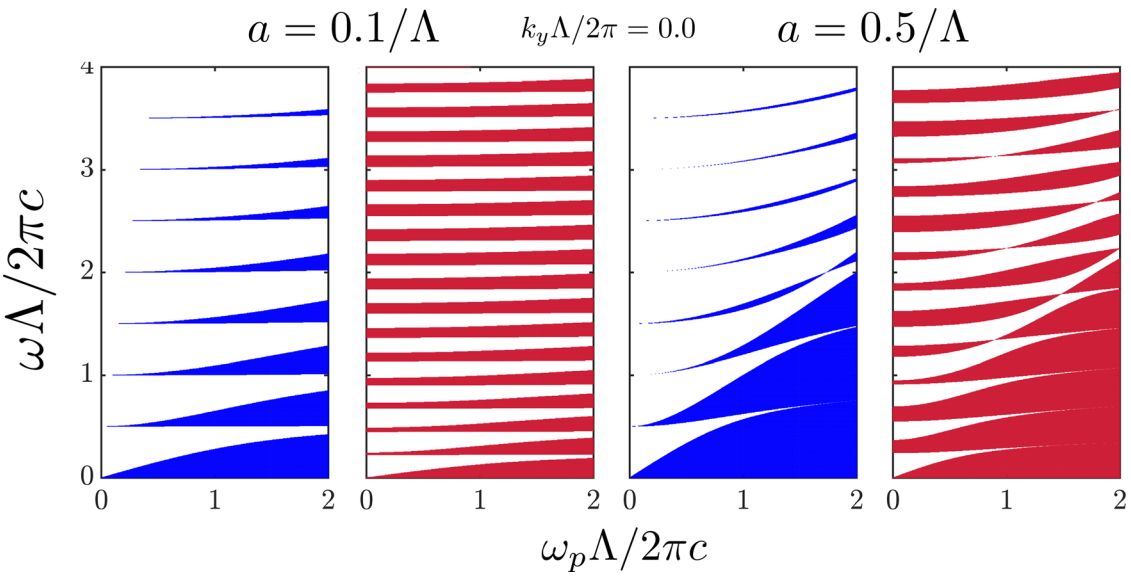


FIG. 7. Bandgap frequency vs. plasma frequency for normal incidence conditions and for $a/\Lambda = 0.1$ (left) and $a/\Lambda = 0.5$ (right) for a 1D plasma photonic crystal. All colored regions are those that are in a bandgap and indicate attenuation. Vacuum (blue) and dielectric $\varepsilon_b = 5$ (red) are shown as the secondary material.

TM polarization.[26] Outside the light line (below the solid horizontal line), we see pass bands emerging for the TM case at low plasma fill fractions. These bands are attributed to the excitation of the asymmetric branch of surface plasmon polaritons[26] at the multi-layer plasma slab/dielectric interface. The transmission is due to the evanescent tunneling of the transverse (z-directed) E-field components that facilitate the coupling of these modes across the PC structure. Like the photonic bandgap modes below the plasma frequency which couple through evanescent fields associated with bulk plasmons, these SPP-facilitated pass bands can be quite narrow and close at higher plasma fill fractions.

Figures 9 and 10 show the wave dispersions (left panels) and corresponding transmittance (right panels) for a finite-sized ($N = 20$) PPC with $\varepsilon_b = 1$, $k_y\Lambda/2\pi = 0.3$, and $a/\Lambda = 0.1$, 0.5, and 0.9 for TE and TM polarizations, respectively. Again, the horizontal black line serves as a demarcation of the light line. At a low plasma fill fraction ($a/\Lambda = 0.1$), the TE case looks similar to that of the normal incidence angle case (top panel of Fig. 5), with the narrow transmission band near $\omega_{p\text{eff}}$ at the upper frequency boundary of the cut-off band. This mode flattens with the increasing fill fraction, with a concomitant decrease in the corresponding transmission bandwidth. This mode is fundamentally the same as that

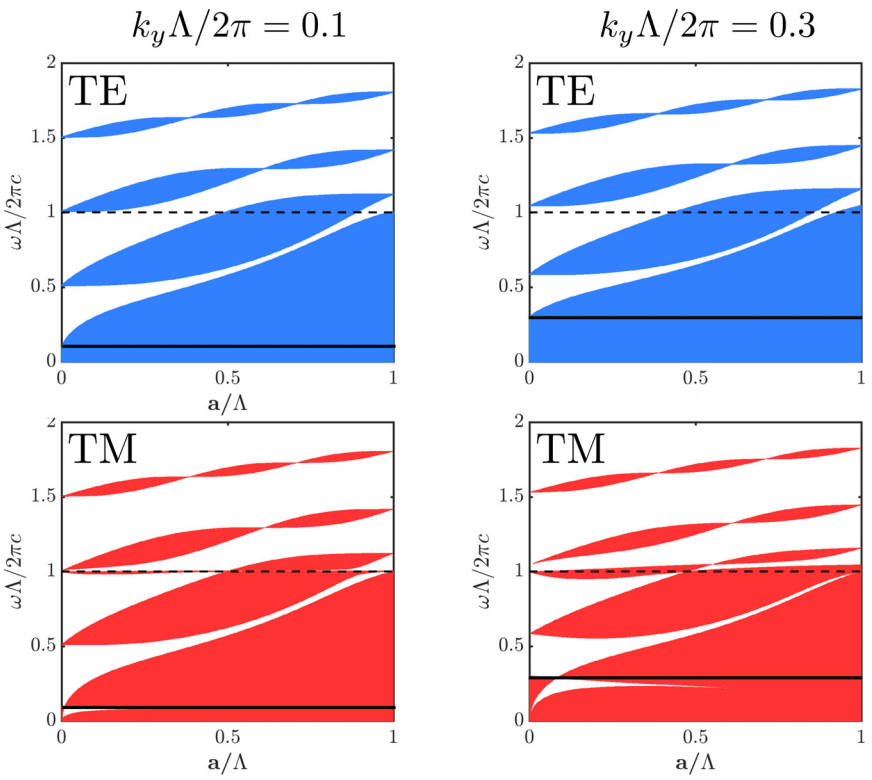


FIG. 8. Bandgap frequency vs. plasma thickness for TE (top) and TM (bottom) polarizations for a 1D plasma photonic crystal with vacuum ($\varepsilon_b = 1$) as the secondary material. All colored regions are frequencies that are in a bandgap. The horizontal dotted line denotes the plasma frequency, with $\omega_p\Lambda/2\pi c = 1$ and $N = \infty$. The horizontal solid line denotes the light line limit.

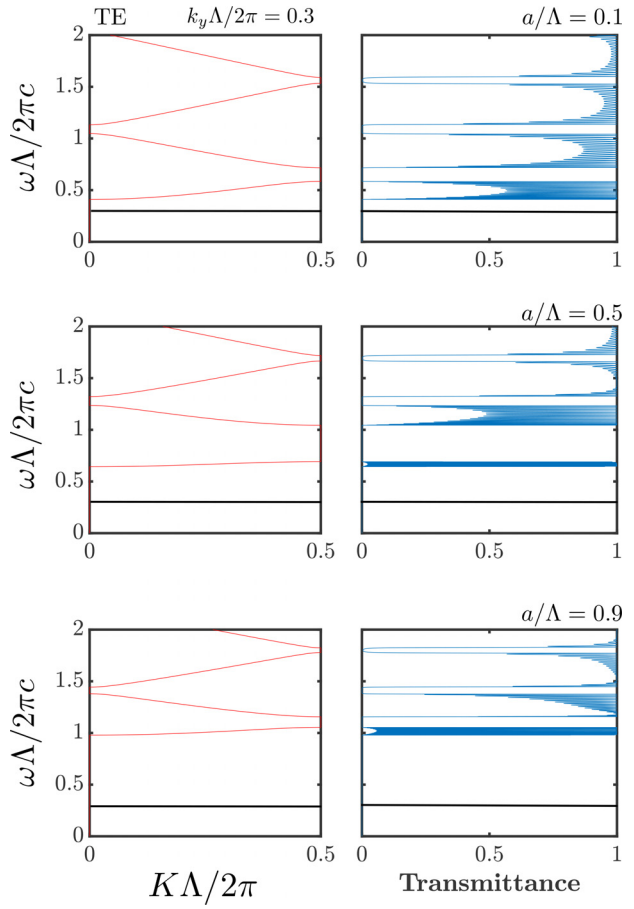


FIG. 9. Dispersion diagrams (left) and transmittance spectra (right) for a 1D plasma photonic crystal in vacuum for N = 20, $a/\Lambda = 0.1$, 0.5, and 0.9, and $\omega_p\Lambda/2\pi c = 1$ for TE polarization.

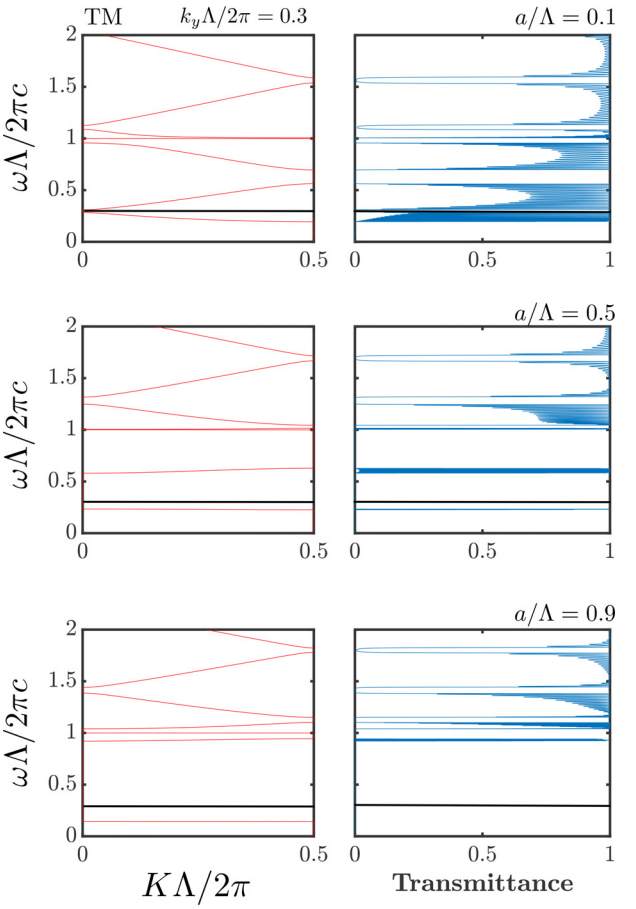


FIG. 10. Dispersion diagrams (left) and transmittance spectra (right) for a 1D plasma photonic crystal in vacuum for N = 20, $a/\Lambda = 0.1$, 0.5, and 0.9, and $\omega_p\Lambda/2\pi c = 1$ for TM polarization.

mode seen at zero incident angles. Its origin is the evanescent wave coupling through the striated layers which are accommodated by bulk plasmons within the plasma slab. At a finite incidence angle, these bulk plasmons, with the E-field polarized in the plane of the slab, facilitate the formation of the inter-facial reflected wave which through successive Bragg scattering result in the high $Q$ inter-band transmission peaks described earlier and in Fig. 6. There are no bands outside of the light line, as TE polarizations cannot couple to surface plasmon polaritons.

The TM polarization case is again different in comparison to the TE case in many respects. First, like the TE polarization, the TM case gives rise to the transmission band in the vicinity of the upper boundary of the cut-off band near $\omega_{peff}$ behaving like the TE case with the increasing fill fraction, becoming quite narrow (flattened dispersion) at high fill fractions, and approaching $\omega_p$ in value. For relatively low fill fractions ($a/\Lambda = 0.1$), the TM case produces a new stop band, which we described above as the anti-node of the Fano resonance, just below $\omega_p$ (see the top right panel of Fig. 10) which lies within the otherwise relatively broad transmission band that extends to just above the plasma frequency, as seen in the TE case. We see that this stop band arises because of the emergence of two new dispersion branches, as seen from the top left panel of Fig. 10, the lower of which is relatively flat, a feature typical of surface plasmon states in plasma photonic crystals,[17] and coincides closely with $\omega_p$. Again, we attribute this SPP mode to the symmetric branch of the surface plasmons propagating along $y$ excited at the plasma-dielectric interface. A very narrow bandgap is defined by where this new flat band and the lower photonic band nearly merge at $K = 0$, in the vicinity of the ENZ condition for the plasma constituent.

At a fill fraction, $a/\Lambda = 0.5$ (center panels of Fig. 10), these new plasmonic bands merge with the upper branch of the lowest transmission band at a frequency of $\omega = \omega_p$. The effect of this merging is to produce a very narrow TM pass

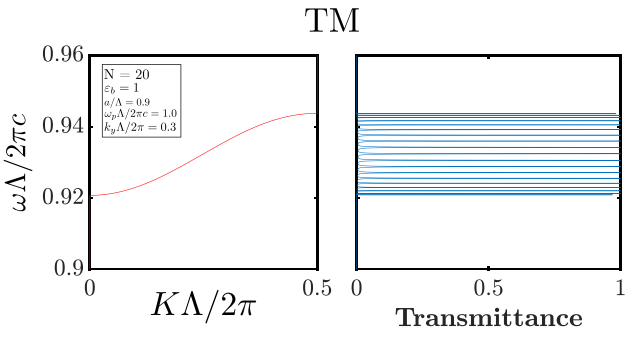


FIG. 11. Zoomed-in dispersion (left) and transmittance spectra (right) for a 1D plasma photonic crystal in vacuum for N = 20, $a/\Lambda = 0.9$, and $\omega_p\Lambda/2\pi c = 1$ for TM polarization showing N-1 transmittance peaks.

band and bandgap in the vicinity of $\omega_p$. At very high fill fractions, $a/\Lambda = 0.9$, the bands separate and the dispersion branch in the vicinity of $\omega_{p,eff}$ shifts towards $\omega_p$ generating a narrow region with two nearly flat branches just below the plasma frequency. The very lowest branch represents the isolated plasmon-facilitated pass band and generates a very narrow transmission band consisting of extremely high-$Q$ inter-band transmission modes, as seen in Fig. 11. Finally, the second major feature seen with TM polarization is the SPP dispersion branch outside of the light line (below the horizontal black line in the figures) due to the asymmetric branch seen in multi-layer metallic structures.[26] At a plasma fill fraction of $a/\Lambda = 0.5$, the transmission band is extremely narrow. At higher fill fractions, this band closes, as discussed earlier.

The differentiation between TE and TM cases for the behavior of these plasmonic modes as the $y$-component wavenumber is varied is depicted in Fig. 12. In these depictions, varying $k_y$ for a fixed incident frequency changes the incident angle $\theta$ since $\sin^{-1}\theta = k_y c/\omega$. The figures highlight the region outside of the light line where $k_y/K > 1$ by the triangular region in the bottom right of each graph. Of course, the two polarizations result in degenerate transmission states when the component wavenumber within the plane $k_y = 0$ (normal incidence). Again, the TE mode behavior is expected, with all the photonic band features shifting towards higher frequency with the increasing angle as the reduction in the wavenumber transverse to the slabs is compensated by an increase in the free space wavenumber (and hence frequency). TM propagation has a distinctly different behavior in three frequency regimes. The first is that the low frequency transmission in the vicinity of the effective plasma frequency does not shift towards higher frequency with increasing $k_y$ but instead remains relatively constant. The second is that the stop band introduced by the new

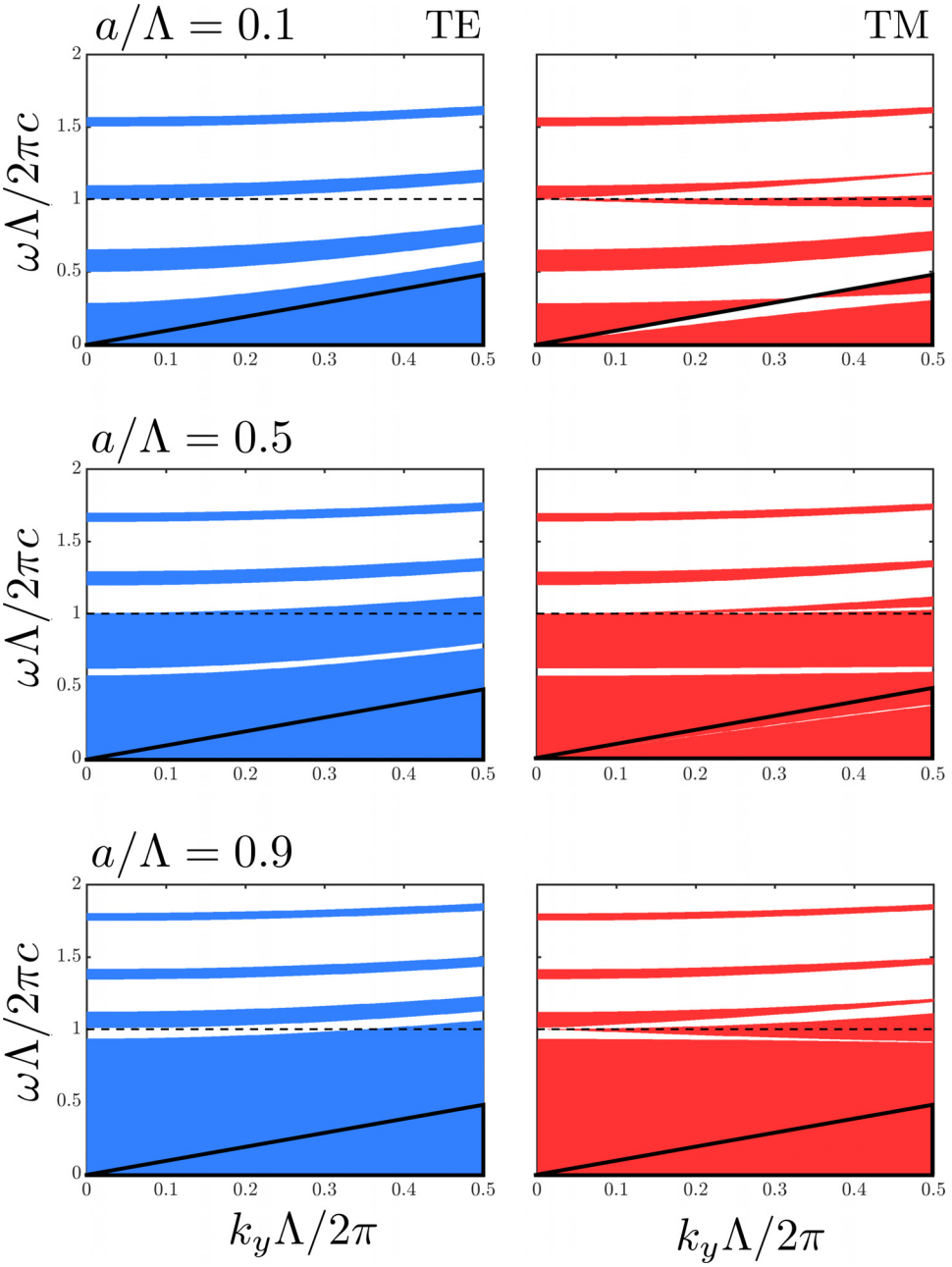


FIG. 12. Bandgap frequency vs. $k_y$ for TE and TM propagation for a 1D plasma photonic crystal ($a/\Lambda = 0.1$, 0.5, and 0.9). All colored regions are those that are in a bandgap. Vacuum ($\varepsilon_b = 1$) is the secondary material. The horizontal dotted line denotes the plasma frequency, and the region with the black triangular line is below the light line.

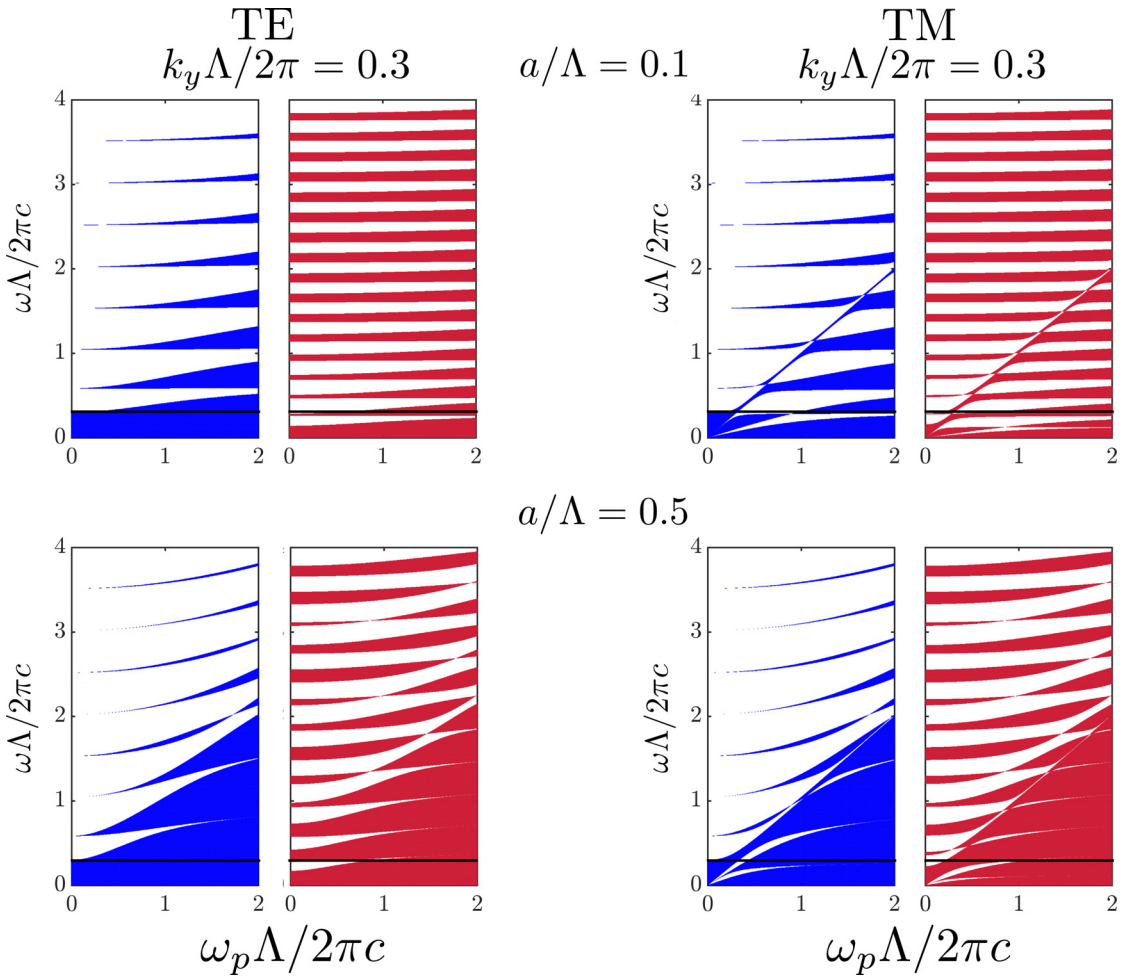


FIG. 13. Bandgap frequency vs. plasma frequency for TE and TM propagation at off incidence ($k_y\Lambda/2\pi = 0.3$) for a 1D plasma photonic crystal. All colored regions are those that are in a bandgap and indicate attenuation, with frequencies below the horizontal black line denoting propagation outside of the light line. Vacuum (blue) and dielectric $\varepsilon_b = 5$ (red) are shown as the secondary material.

propagation branches described above (in the vicinity of $\omega_p$) appears clearly for low fill fractions ($a/\Lambda = 0.1$) across all values of $k_y$. At plasma fill fractions of $a/\Lambda = 0.5$, it merges with the first photonic bandgap centered below the plasma frequency, resulting in a very narrow transmission band at higher values of $k_y$. At very high fill fractions ($a/\Lambda = 0.9$), as we saw from Fig. 10, the dispersion branches once again separate and open up new stop and pass bands near $\omega_p$. The third feature that distinguishes TM from TE propagation is the presence of the very narrow asymmetric mode SPP-facilitated transmission band, which appears for fill fractions of $a/\Lambda \leq 0.5$.

The bandgap variation with $\omega_p$ (or plasma density) for both TE and TM polarizations is depicted in Fig. 13. The most striking feature seen at low plasma fill fractions ($a/\Lambda = 0.1$) in this figure is the strong presence of the plasmonic stop band near $\omega_p$ for the TM case that is completely absent in the TE case. At higher fill fractions ($a/\Lambda = 0.5$), the stop bands become pass bands and photonic bands below the plasma frequency begin to close significantly. The asymmetric surface plasmon mode is visible as the lowest frequency band outside of the light line (below the solid horizontal line). It is important to emphasize that these plasmonic features, particularly that in the vicinity of the plasma frequency, are tunable by variation in the plasma density and can be quite narrow in some cases.

Finally, the E and H-fields (real and imaginary components for all three directions) associated with the highly tunable TM plasmonic stop band just below and above the plasma frequency for $a/\Lambda = 0.3$ and $\omega\Lambda/2\pi c = 0.97$ (lower panels) and $\omega\Lambda/2\pi c = 1.01$ (upper panels) are shown in Fig. 14. For frequencies just above the plasma frequency, the incident EM wave appears to couple into an extended waveguide mode within the dielectric layer. At just below the plasma frequency, the evanescent waves couple into waveguide modes that extend deeper into the structure with an envelope that decays exponentially decaying over a length equal to about 1/3rd of the $N = 20$ 1D PPC structure. The field structure for TE modes (not shown) is unremarkable, reflecting no attenuation within the structure and strong transmission. The behavior changes dramatically about the $\varepsilon_p = 0$ condition, a region where there is strong dispersion and where the external field excites the symmetric branch of the interfacially propagating SPPs. The study of artificial layered structures incorporating such ENZ materials is currently a field of growing activity[27,28] and affords tunability by varying plasma density.

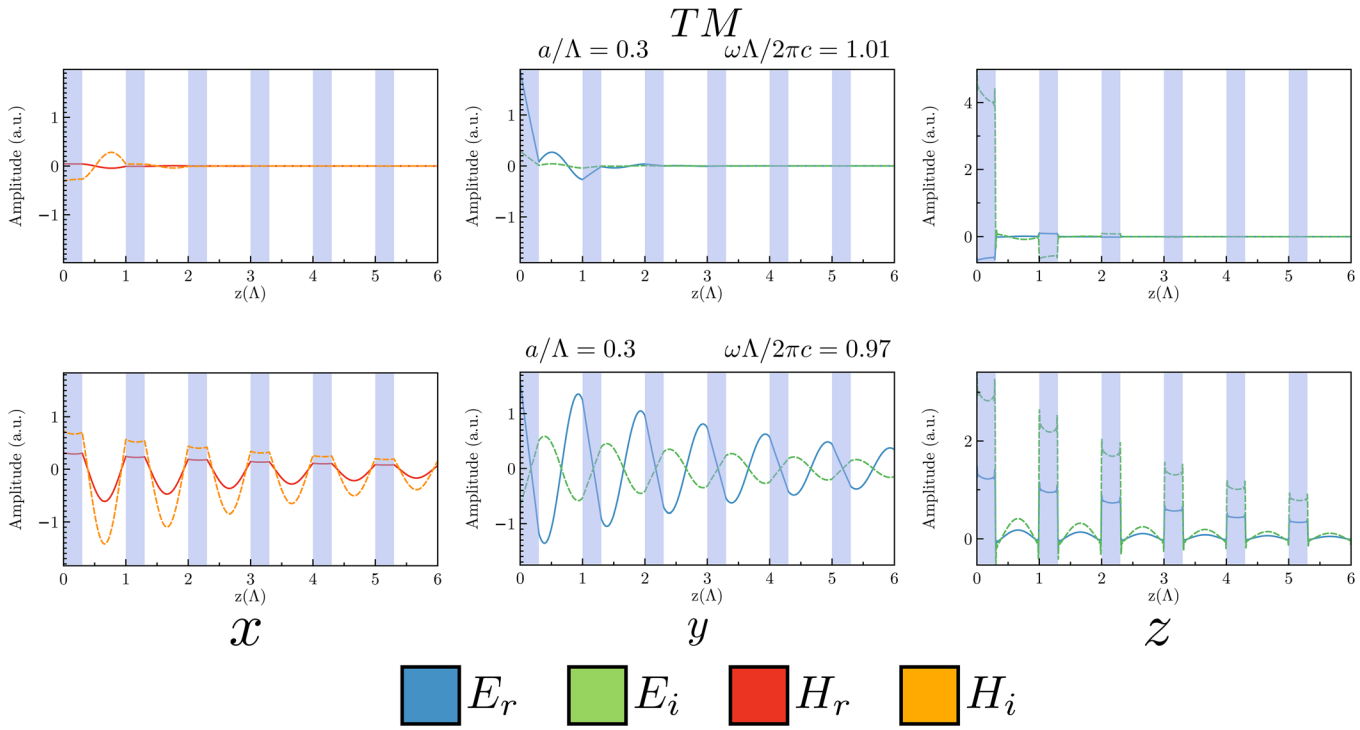


FIG. 14. Cross-sectional electric and magnetic fields are shown for specific frequencies of interest above and below the plasma frequency, with TM polarization at an incident angle of 17° calculated using S4.

## IV. CONCLUSION

In conclusion, we have presented bandgap renderings for a 1D PPC for normal incident EM waves as well as for oblique incident waves of TE and TM polarization. Above the effective plasma frequency, $\omega_{p\text{eff}}$, the bandgap structure for TE polarization is typical of that associated with all-dielectric PCs, with the exception that PPCs introduce a cut-off band that forbids propagation below $\omega_{p\text{eff}}$, as expected. The formation of typical photonic crystal bandgaps and associated transmission bands below $\omega_p$ is facilitated by the tunneling of the EM wave through bulk plasmon evanescent wave coupling between the plasma and vacuum/dielectric layers. The location of these photonic crystal bands shifts slightly towards higher frequency and broadens with increasing plasma density. TM wave propagation is generally similar in this regard; however, we also see the emergence of surface plasmonic features which introduce propagation bands at low frequency outside of the light line and stop bands within the propagation bands in the vicinity of $\omega_p$ where $\varepsilon_p = 0$. These two features coincide with the excitation of asymmetric and symmetric branches of SPPs propagating at the plasma-dielectric interfaces. The latter of these appears to interfere with the photonic crystal Bragg resonance when conditions are such that the plasma frequency is in the vicinity of the lattice frequency, i.e., $\omega_p \approx 2\pi$ c/Λ. The stop band that appears near $\omega_p$ is attributed to the anti-node in the Fano resonance. These plasmonic responses provide a new opportunity for tunable, narrow transmission features that can be used for engineering PPC devices.

A significant challenge moving forward is to generate, experimentally, a truly 1D PPC based on striated plasma layers to confirm the presence of these features and to unambiguously demonstrate their tunability. In practice, the plasma is likely to be somewhat non-uniform, and the conditions will be such that there may be significant wave dissipation due to electron collisional damping. Both these have been investigated for a limited range of conditions in previous work.[21,29]

## ACKNOWLEDGMENTS

This work was supported by a Multidisciplinary University Research Initiative from the Air Force Office of Scientific Research with M. Birkan as the program manager. B.W. was partially supported by a National Defense Science and Engineering Graduate Fellowship. B.W. would also like to thank Dr. Victor Liu for technical support and $S^4$ simulation discussion.

[1]J. D. Joannopoulos, S. G. Johnson, J. N. Winn, and R. D. Meade, *Photonic Crystals Molding the Flow of Light*, 2nd ed. (Princeton University Press, Princeton, NJ, 2008).
[2]H. Hitoshi and A. Mase, J. Plasma Fusion Res. **80**, 89 (2004).
[3]O. Sakai and K. Tachibana, Plasma Sources Sci. Technol. **21**, 013001 (2012).
[4]O. Sakai, T. Sakaguchi, and K. Tachibana, J. Appl. Phys. **101**, 073304 (2007).
[5]B. Wang and M. A. Cappelli, Appl. Phys. Lett. **108**, 161101 (2016).
[6]B. Wang and M. A. Cappelli, Appl. Phys. Lett. **107**, 171107 (2015).
[7]J. Gregório, S. Parsons, and J. Hopwood, Plasma Sources Sci. Technol. **26**, 02LT03 (2017).
[8]L. Shiveshwari and P. Mahto, Solid State Commun. **138**, 160 (2006).
[9]B. Guo, Phys. Plasmas **16**, 043508 (2009).
[10]L. Zhang and J. T. Ouyang, Phys. Plasmas **21**, 103514 (2014).
[11]S. Shukla, S. Prasad, and V. Singh, Phys. Plasmas **22**, 022122 (2015).
[12]L. Qi, Z. Yang, F. Lan, X. Gao, and Z. Shi, Phys. Plasmas **17**, 042501 (2010).
[13]S. Prasad, Y. Sharma, S. Shukla, and V. Singh, Phys. Plasmas **23**, 032123 (2016).

[14]M. Scalora, M. J. Bloemer, A. S. Pethel, J. P. Dowling, C. M. Bowden, and A. S. Manka, J. Appl. Phys. **83**, 2377 (1998).
[15]S. Feng, J. M. Elson, and P. L. Overfelt, Opt. Express **13**, 4113 (2005).
[16]A. A. Orlov, S. V. Zhukovsky, I. V. Iorsh, and P. A. Belov, Photonics Nanostruct.- Fundam. Appl. **12**, 213 (2014).
[17]O. Sakai and K. Tachibana, IEEE Trans. Plasma Sci. **35**, 1267 (2007).
[18]L. Shiveshwari, Opt.-Int. J. Light Electron Opt. **122**, 1523 (2011).
[19]M. Klein, T. Tritschler, M. Wegener, and S. Linden, Phys. Rev. B **72**, 115113 (2005).
[20]T. Naito, O. Sakai, and K. Tachibana, Appl. Phys. Express **1**, 066003 (2008).
[21]W. Fan and L. Dong, Phys. Plasmas **17**, 073506 (2010).
[22]P. Yeh, A. Yariv, and C.-S. Hong, J. Opt. Soc. Am. **67**, 423 (1977).
[23]C.-J. Wu, T.-J. Yang, C. C. Li, and P. Y. Wu, Prog. Electromagn. Res. **126**, 521 (2012).
[24]V. Liu and S. Fan, Comput. Phys. Commun. **183**, 2233 (2012).
[25]J. A. Monsoriu, R. A. Depine, M. L. Martínez-Ricci, and E. Silvestre, Opt. Express **14**, 12958 (2006).
[26]E. Economou, Phys. Rev. **182**, 539 (1969).
[27]J. Gao, L. Sun, H. Deng, C. J. Mathai, S. Gangopadhyay, and X. Yang, Appl. Phys. Lett. **103**, 051111 (2013).
[28]P. Ginzburg, F. J. R. Fortuño, G. A. Wurtz, W. Dickson, A. Murphy, F. Morgan, R. J. Pollard, I. Iorsh, A. Atrashchenko, P. A. Belov, Y. S. Kivshar, A. Nevet, G. Ankonina, M. Orenstein, and A. V. Zayats, Opt. Express **21**, 14907 (2013).
[29]L. Qi, C. Li, G. Fang, and X. Gao, Plasma Sci. Technol. **17**, 4 (2015).